

An Improved Two-Phase Flow Model of the Compression of Paste Briquettes – Elkem

1 Foreword

As a supplementary problem for the 1998 European Study Group with Industry, ELKEM ASA wished to reconsider the paste briquette compression model first proposed at the 1997 meeting. Much of the detailed modelling involved is similar to the previous report, contained in Budd (1997), but there are important differences in some respects which are highlighted below. Some general detail has also been retained in this report so that it may be read as a self-contained document.

2 Introduction

Continuous carbon electrodes are widely used in electric smelting furnaces. Their purpose is to conduct the large currents required by the smelting process to the centre of the furnace. Inevitably, the electrodes are gradually consumed under the extreme heat of the furnace, at a rate of around 0.5 – 1 m/day. A great deal of effort has gone into finding efficient and practical ways of recharging the electrodes. A discussion of some typical industrial configurations and some related references are given in Fitt & Howell (1998).

Here we are concerned with a proposed new technology that involves adding “briquettes” to the top of the electrode, rather than large, unwieldy sections. The briquettes in question are small bricks (typically around $10 \times 6 \times 4$ cm) of a material normally referred to as “paste”, which comprises small particles of calcined anthracite bound together by a mixture of tar and pitch. For the purposes of this paper, paste is assumed to behave as a Newtonian liquid, albeit with a strongly temperature-dependent viscosity. At room temperature, the briquettes are solid; they soften and flow as the

temperature increases up to about 200–250°C. As the temperature is further increased, the anthracite particles begin to react and bind — a process known as “baking” that results in the viscosity beginning to rise again. At around 400°C the viscosity of the paste increases rapidly and it becomes solid at 500°C.

The idea of the new process is as follows. As the briquettes propagate slowly down the electrode, they heat up and begin to flow. The air is gradually squeezed out by the weight of the briquettes above. As the temperature increases further down the electrode, the compressed paste/air mixture bakes and a solid “self-baking” electrode is formed.

Vital to the success of the process is that the baked electrode should be both mechanically strong and a good electrical conductor. These properties are closely related to the amount of air that is left in the electrode when it bakes, and a clear understanding of the way in which air is expelled is required so that optimal process conditions can be determined. To gain such understanding, Elkem have devised the experiment shown schematically in figure 1. A cylinder of radius a is filled with briquettes up to a height L , and the top is loaded with a mass M . The piston and sides of the container are perforated in such a way that air can escape but paste cannot. The cylinder is then heated up to a constant temperature of about 100°C, and over a period of 5–6 hours the position of the top of the piston is monitored.

In Budd (1997), a two-phase flow model was proposed for the flow of the paste/air mixture. In Fitt & Howell (1998) the model was applied to both the experiment and a simplified electrode configuration, and some encouraging results were obtained. However, it was observed that the model tended to predict rather more rapid expulsion of air than was observed in the experiment. In this paper we propose a refined model that (*i*) relaxes a simplifying assumption made in Budd (1997). and (*ii*) gives somewhat better agreement with experimental results. In section 3 we present the general two-phase model that might be solved numerically in a realistic electrode geometry. In section 4 we use a one-dimensional version of the model to simulate the experiment.

3 Two-phase flow model

We begin this section by outlining the basic two-phase flow model for the paste/air mixture derived in Budd (1997). We denote the air and paste phases by the suffices 1 and 2 respectively. The relevant dimensional parameters for each phase are the density (ρ_i), dynamic viscosity (μ_i), specific heat (c_{pi}) and thermal conductivity (k_i), whilst the velocity, pressure and

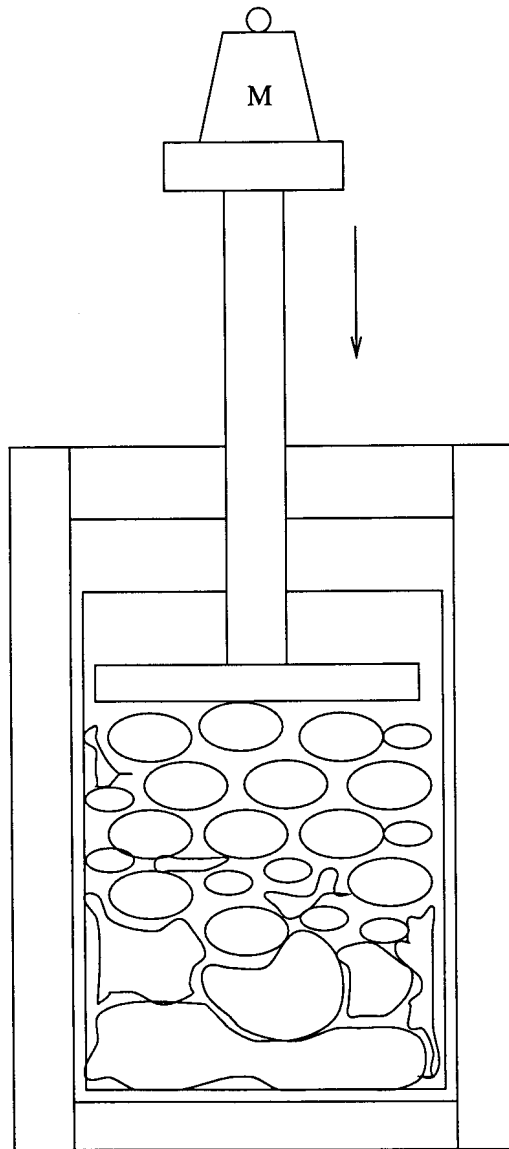


Figure 1: Experimental device for measurement of air expulsion from compressed briquettes

temperature in phase i are denoted by \mathbf{u}_i , p_i and T_i respectively. Finally, α denotes the volume fraction of paste (and thus $1 - \alpha$ denotes the volume fraction of air).

3.1 The general equations

Using order-of-magnitude arguments (see Fitt & Howell (1998) for details), the most general two-phase flow equations may be simplified to the following. First we have flow equations for the paste

$$\alpha_t + \nabla \cdot (\alpha \mathbf{u}_2) = 0, \quad (1)$$

$$\alpha \nabla p_2 = \nabla \cdot (\alpha \mu_2 [\nabla \mathbf{u}_2 + \nabla \mathbf{u}_2^T]) - \rho_2 g \alpha \mathbf{k} + \mathbf{D}, \quad (2)$$

whilst for the air

$$-\alpha_t + \nabla \cdot ((1 - \alpha) \mathbf{u}_1) = 0, \quad (3)$$

$$(1 - \alpha) \nabla p_1 = -\mathbf{D}. \quad (4)$$

The flow of the two phases is coupled through the interactive drag term \mathbf{D} . The leading-order heat-flow equations are

$$(\rho_2 c_{p2} \alpha T_2)_t + \nabla \cdot (\rho_2 c_{p2} \alpha T_2 \mathbf{u}_2) = \nabla \cdot (k_2 \alpha \nabla T_2), \quad (5)$$

$$0 = \nabla \cdot (k_1 (1 - \alpha) \nabla T_1). \quad (6)$$

Notice that the only coupling between (5), (6) and (1–4) is through the viscosity μ_2 , which we shall assume henceforth to be a known function of T_2 .

To close the system (1–6) a constitutive equation for \mathbf{D} and a relationship between p_1 and p_2 are required. In both Budd (1997) and Fitt & Howell (1998), the simplest closure assumption $p_1 = p_2$ was employed. The closure problem for two-phase flow is difficult, and this relationship is frequently employed. It is known, however, that in many cases it may lead to analytical and numerical difficulties and to unrealistic predictions. In the following subsection we therefore examine ways in which this frequently-used approximation might be improved.

3.2 The relation between the pressures

We begin by examining two particularly simple geometries in which the slow-flow equations may readily be solved. Consider first a shrinking cylinder of radius $a(t)$ containing air at pressure p_1 in a viscous liquid at pressure p_2 . p_1 is assumed to be constant (the pores have not yet closed and so any increase in gas pressure is instantly relieved by flow) whilst p_2 is notionally the “liquid

pressure” (the pressure in the liquid on a microscopic scale but far away from the cylinder). Assuming that $\mathbf{u}_2 = u_2 \mathbf{e}_r$ where \mathbf{e}_r is a unit vector in the radial direction, in the viscous fluid conservation of mass gives

$$(ru_{2r})_r = 0.$$

Since $u = \dot{a}$ at $r = a$ we therefore have $u_2 = a\dot{a}/r$. The Stokes flow equation is

$$p_{2r} = \mu_r \left[\frac{(ru_{2r})_r}{r} - \frac{u_2}{r^2} \right]$$

and thus $p_{2r} = 0$ and p_2 is a function of time alone. Balancing the normal stresses on $r = a$ gives

$$-p_1 = -p_2 + 2\mu_2 u_{2r}$$

and thus

$$p_2 - p_1 = -\frac{2\mu_2 \dot{a}}{a}, \quad (7)$$

relating the pressure difference to the rate at which the cylinder shrinks.

Now consider the same problem for a sphere of radius $a(t)$. Again, the Stokes equations may be solved exactly, revealing that

$$p_2 - p_1 = -\frac{4\mu_2 \dot{a}}{a}. \quad (8)$$

In either case we may relate a to the effective volume fraction of paste by considering a ‘control volume’ of paste and air that is small compared to the experimental dimensions, but large compared to an air-filled pore. We find that

$$\frac{1 - \alpha}{\alpha} \propto \begin{cases} a^2 & \text{(cylinder),} \\ a^3 & \text{(sphere),} \end{cases} \quad (9)$$

The constant of proportionality (which will in any case not appear in expressions for the pressure difference) depending upon the geometrical details of exactly how the air-filled void is contained in an elementary region of viscous fluid.

In general, therefore, we expect the pressure difference across the paste/air interface to be of the form

$$p_2 - p_1 = \frac{k\mu_2 \dot{a}}{\alpha(1 - \alpha)}, \quad (10)$$

where the constant k depends on the local morphology of the interface; as shown above, in the case of a cylinder $k = 1$ while for a sphere $k = 4/3$. These two examples suggest that k should not vary too much as the interface

evolves. Henceforth we adopt (10) as a constitutive relation between p_1 and p_2 , and assume that k remains constant (and known) during any experiment. Notice that the relation used by Fitt & Howell (1998) is recovered by setting $k = 0$.

3.3 The two flow regimes

It remains to determine the drag term D . The situation depends crucially on whether the air phase is in “**Regime I**”, where the pores are largely mutually connected, or “**Regime II**” where air is dispersed through the paste in isolated packets. Evidently when the briquettes are solid regime I applies; as they soften and begin to flow, the general picture is of a network of pores that slowly fill with melting paste. As long as the pores remain open (*i.e.*, regime I still applies), an order-of-magnitude argument (see Fitt & Howell (1998) for full details) shows that $D \approx \mathbf{0}$. It follows that $p_1 \approx \text{const.} = 0$ (without loss of generality) and so we obtain the system

$$\alpha_t + \nabla \cdot (\alpha \mathbf{u}_2) = 0, \quad (11)$$

$$\alpha \nabla p_2 = \nabla \cdot (\alpha \mu_2 [\nabla \mathbf{u}_2 + \nabla \mathbf{u}_2^T]) - \rho_2 g \alpha \mathbf{k}, \quad (12)$$

with

$$p_2 = -\frac{k \mu_2 \nabla \cdot \mathbf{u}_2}{1 - \alpha}, \quad (13)$$

and an associated energy equation

$$(\rho_2 c_{p2} \alpha T_2)_t + \nabla \cdot (\rho_2 c_{p2} \alpha T_2 \mathbf{u}_2) = \nabla \cdot (k_2 \alpha \nabla T_2). \quad (14)$$

At some stage during the flow, the pores close off to form separate and unconnected packets or bubbles, whereupon regime II applies. We assume that this occurs at a given value of α , say $\alpha = \alpha_c$. Once we are in regime II the air cannot flow so α must remain at this critical value. However, since the air phase is now dispersed rather than continuous, the assumption that p_1 is constant is no longer justified, and in general we have the system

$$\alpha = \alpha_c, \quad (15)$$

$$\nabla \cdot \mathbf{u}_2 = 0, \quad (16)$$

$$\nabla p_2 = \alpha_c \nabla \cdot (\mu_2 [\nabla \mathbf{u}_2 + \nabla \mathbf{u}_2^T]) - \rho_2 g \alpha_c \mathbf{k}, \quad (17)$$

$$(\rho_2 c_{p2} T_2)_t + \nabla \cdot (\rho_2 c_{p2} T_2 \mathbf{u}_2) = \nabla \cdot (k_2 \nabla T_2), \quad (18)$$

where p_2 is no longer known *a priori*.

Within our two-phase framework, there is no way to predict α_c : it must be found from either experiments or by direct numerical simulation of the transition between regimes I and II. To simplify matters we neglect the details of the transition and simply switch abruptly from regime I to regime II when α reaches α_c , treating α_c as a known paste property.

4 Analysis of the experiment

4.1 The one-dimensional model

We now examine the governing equations (11)-(18) for one-dimensional flow where all variables depend only upon z , the vertical distance from the base of the cylinder, and time. For simplicity the subscript 2 will be dropped from the variables referring to the paste. A detailed description of the experiment is given in Fitt & Howell (1998). Here we simply examine how the one-dimensional analysis carried out there is affected by the new relationship (13) between p_1 and p_2 . We use the same nondimensionalisation as Fitt & Howell (1998), namely

$$z = L\tilde{z}, \quad s = L\tilde{s}, \quad p = \frac{Mg}{2\pi a^2}\tilde{p}, \quad w = \frac{MgL}{2\pi a^2\mu_{20}}\tilde{w}, \quad t = \frac{2\pi a^2\mu_{20}}{Mg}\tilde{t}, \quad \mu_2 = \mu_{20}\tilde{\mu}_2$$

where μ_{20} is a representative paste dynamic viscosity. Dropping the tildes for convenience, the non-dimensional versions of (11)-(13) (the governing equations for regime I) become

$$\alpha_t + (\alpha w)_z = 0, \quad \alpha p_z = (2\mu_2\alpha w_z)_z - 2g^*\alpha, \quad (19)$$

where

$$p = -\frac{k\mu_2 w_z}{1-\alpha}. \quad (20)$$

Here the dimensionless parameter g^* is the ratio of the weight of the briquettes to that of M :

$$g^* = \frac{\pi a^2 \rho_2 L}{M}. \quad (21)$$

In the experiments carried out thus far g^* is fairly small (around 0.3), and Fitt & Howell (1998) obtained a good approximation by considering the limit $g^* \rightarrow 0$. This limit will be investigated in section 4.2.

Note that the equations (19) and (20) apply only in regime I, that is only for $\alpha < \alpha_c$. When α reaches α_c we simply have

$$\alpha = \alpha_c, \quad w = 0. \quad (22)$$

The boundary conditions are

$$\left. \begin{aligned} \alpha(p - 2\mu_2 w_z) &= 2 \\ w &= \dot{s} \\ w &= 0 \end{aligned} \right\} \begin{aligned} z &= s(t), \\ z &= 0, \end{aligned} \quad (23)$$

where the position of the moving piston is denoted by $z = s(t)$, and the initial conditions are

$$\alpha = \alpha_0, \quad s = 1 \quad \text{at } t = 0. \quad (24)$$

The viscosity μ_2 is assumed to be a known function of temperature T , which in general must be found from a coupled heat-transfer problem. However, if the heating is assumed to be uniform in space, then μ_2 will be a function only of t . This simplifies matters considerably since the transformation

$$w^* = \mu_2(t)w, \quad t^* = \int_0^t \frac{dt'}{\mu_2(t')} \quad (25)$$

yields the same problem with $\mu_2 \equiv 1$. We therefore concentrate on the isothermal case $\mu_2 = 1$ for the moment, safe in the knowledge that temperature variations that are independent of z may be included later by rescaling time appropriately.

The problem defined by (19)-(24) must, in general, be solved numerically, and a stratagem for doing this is outlined in the appendix. We note however, that there are some limits in which analytical progress may be made: these are now discussed.

4.2 The limit $g^* \rightarrow 0$

If we assume that the briquettes are much lighter than the mass M and therefore set $g^* = 0$, then on physical grounds and by inspection of the equations (19) we deduce that α is spatially uniform and depends only upon time. Setting $\mu_2 = 1$ for simplicity (see above remarks) the velocity is therefore given by

$$w = -\frac{\dot{\alpha}z}{\alpha},$$

whereupon the second equation of (19) gives that p is a function of time alone. Eliminating the pressure between (20) and the first boundary condition of (23) now gives an ordinary differential equation for α . Solving this, we obtain an implicit equation for $\alpha(t)$,

$$t = \alpha - \alpha_0 + \frac{k}{2} \log \left(\frac{1 - \alpha_0}{1 - \alpha} \right), \quad (26)$$

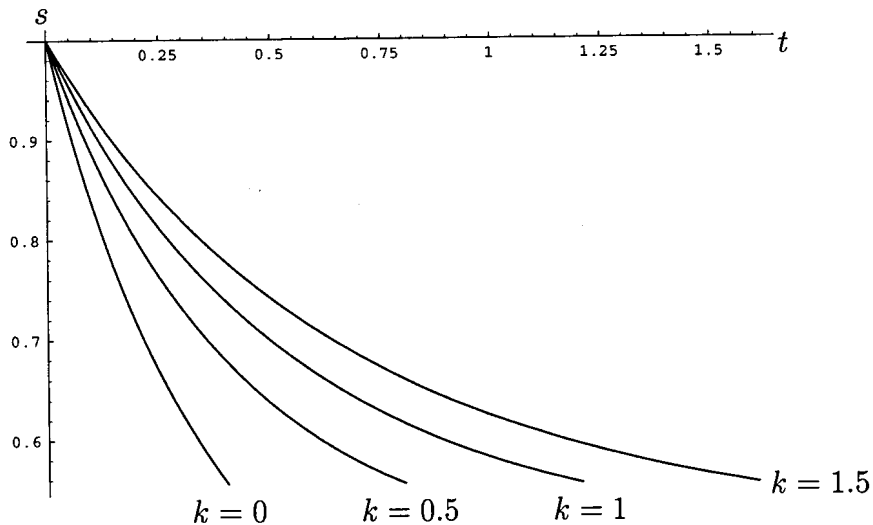


Figure 2: The free boundary $s(t)$ versus t for $k = 0, 0.5, 1, 1.5$. Here $g^* = 0$, $\alpha_0 = 0.5$ and $\alpha_c = 0.9$.

while the free boundary $s(t)$ being given simply by

$$s = \frac{\alpha_0}{\alpha}. \quad (27)$$

The solution (26) predicts (as would be expected) a monotonic increase of α , with

$$\alpha \sim 1 - e^{-2t/k} \quad \text{as } t \rightarrow \infty.$$

This ceases to be valid when α reaches α_c , from which point α remains fixed at that value. Notice that, with α spatially uniform, the transition from regime I to regime II takes place simultaneously everywhere.

In figure 2 we plot the free boundary $s(t)$ for several values of k , setting $\alpha_0 = 0.5$, $\alpha_c = 0.9$. Notice that increasing k broadly has the effect of slowing down the process, particularly towards the end of the experiment. This is encouraging since the solution with $k = 0$ was found by Fitt & Howell (1998) to predict rather more rapid compression than had been observed in experiments.

4.3 The case $k = 0$

The main point of this study is to consider cases where $k \neq 0$. A closed-form solution is available, however, for general g^* when $k = 0$, and is of use for numerical validation purposes. The details of the solution in this special case

may be found in Fitt & Howell (1998); here we just quote the relevant results. (Once again, we set $\mu_2 = 1$ without loss of generality.)

So long as regime I applies throughout the paste/air mixture, the void fraction and piston height are given by

$$\alpha = [\alpha_0(1 + g^*t) + t] e^{-g^*zt}, \quad (28)$$

$$s = \frac{1}{g^*t} \log \left(\frac{\alpha_0(1 + g^*t) + t}{\alpha_0 + t} \right). \quad (29)$$

The velocity w may also be determined if desired. This solution ceases to be valid when α reaches α_c . This occurs first at $z = 0$, $t = t_c$, where

$$t_c = \frac{\alpha_c - \alpha_0}{1 + \alpha_0 g^*}.$$

For $t > t_c$ there is a second free boundary $z = l(t)$ such that Regime I applies in $z > l$ and Regime II in $z < l$. The solutions for α , s and l when $l < z \leq s$ are now

$$\alpha = \alpha_c \exp \left(\frac{\alpha_0 - \alpha_c + (1 + \alpha_0 g^*)t - \alpha_c g^* z t}{\alpha_c} \right), \quad (30)$$

$$s = \frac{1 + \alpha_0 g^*}{\alpha_c g^*} - \frac{\alpha_c - \alpha_0}{\alpha_c g^* t} + \frac{1}{g^* t} \log \left(\frac{\alpha_c}{\alpha_0 + t} \right), \quad (31)$$

$$l = \frac{(1 + \alpha_0 g^*)(t - t_c)}{\alpha_c g^* t} \quad (32)$$

and again w may be determined if desired.

The whole process stops when $l = s$, so that $\alpha = \alpha_c$ everywhere. This occurs at time $t = t_f$ where

$$t_f = \alpha_c - \alpha_0.$$

It is worth noticing that t_f is independent of g^* . This is because t_f denotes the time for the mixture right at the top of the cylinder (which feels only the weight of M and not of any paste) to be crushed down to a fraction α_c . This is further evidence that the important characteristics of the process are captured by the $g^* \rightarrow 0$ limit.

4.4 Numerical solution

We now turn to the most general case where neither of k or g^* is non-zero. For full details of the numerical procedure that was used, the reader is referred to the appendix. In all the computations to follow we use the sample values

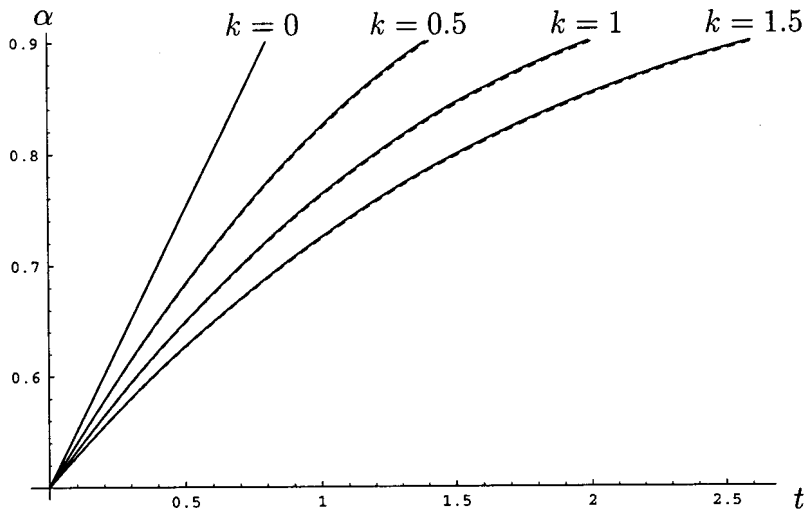


Figure 3: Paste volume fraction α versus z for increasing t (timestep between plots = 0.05). Here $k = 0$, $g^* = 1$, $\alpha_0 = 0.5$, $\alpha_c = 0.9$, so that $t_f = 0.4$, $t_c \approx 0.2667$. In each case, the solid line is computed numerically, whilst the dashed line is the exact solution.

$\alpha_0 = 0.5$, $\alpha_c = 0.9$. First the numerical scheme was tested by computing $\alpha(z, t)$ for $k = 0$, $g^* = 1$, for which we have the exact solution (28, 30). In figure 3 α is plotted against z for increasing values of t (with increment 0.05 time units). In each case the computed solution is represented by a solid line, whilst a dashed line is used for the exact solution — in this plot they are almost completely indistinguishable. Notice the stagnant zone with $\alpha = \alpha_c$ that appears near $z = 0$ for $t > t_c \approx 0.2667$. The whole process finishes with $\alpha = \alpha_c$ everywhere at $t = t_f = 0.4$.

In figure 4 we show the corresponding plot with $g^* = 1$, $k = 1$. Qualitatively, the evolution of α is similar to (though rather slower than) the case when $k = 0$: the time t_f at which the process finishes is increased by a factor of about three.

In figure 5 the effect of varying k is examined by plotting the two free boundaries $s(t)$ and $l(t)$ against t with g^* fixed at 1 for various values of k . As before, the exact solution for $k = 0$ is shown as a dashed line; the accuracy of the numerical scheme is confirmed by the fact that the exact and numerical solutions are again indistinguishable. The most important conclusion that can be drawn from figure 5 is that the time taken for the air to be expelled varies quite dramatically with k . This strongly suggests that whilst the $k = 0$ solution used for comparison purposes in Fitt & Howell (1998) is qualitatively correct, it is unlikely to give good quantitative agreement with experimental

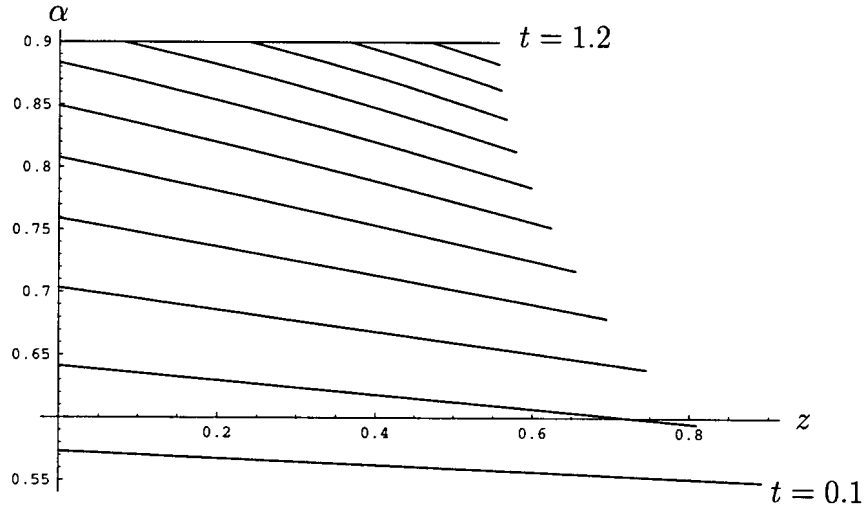


Figure 4: Paste volume fraction α versus z for increasing t (timestep between plots = 0.1). Here $k = 1$, $g^* = 1$, $\alpha_0 = 0.5$, $\alpha_c = 0.9$, so that $t_f \approx 1.2$, $t_c \approx 0.76$.

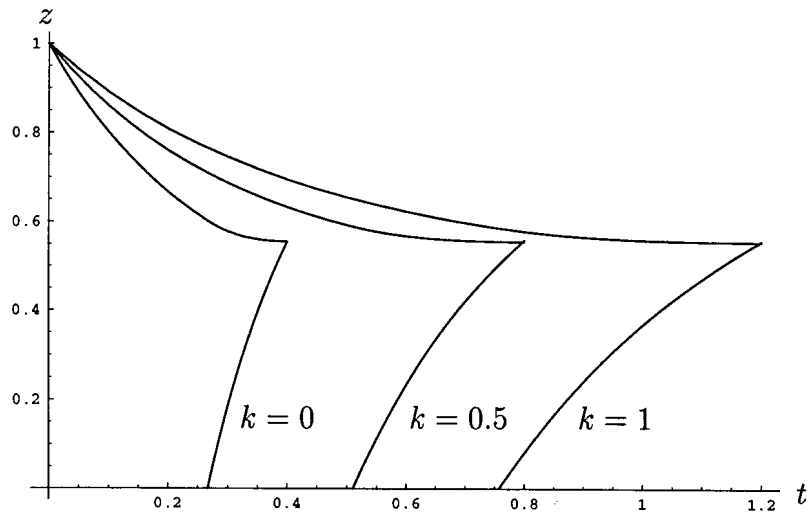


Figure 5: Height of paste $s(t)$ and free boundary $l(t)$ (dividing regimes I and II) versus t for $g^* = 1$, $\alpha_0 = 0.5$, $\alpha_c = 0.9$ and $k = 0, 0.5, 1$. The dashed line shows the exact solution for $k = 0$.

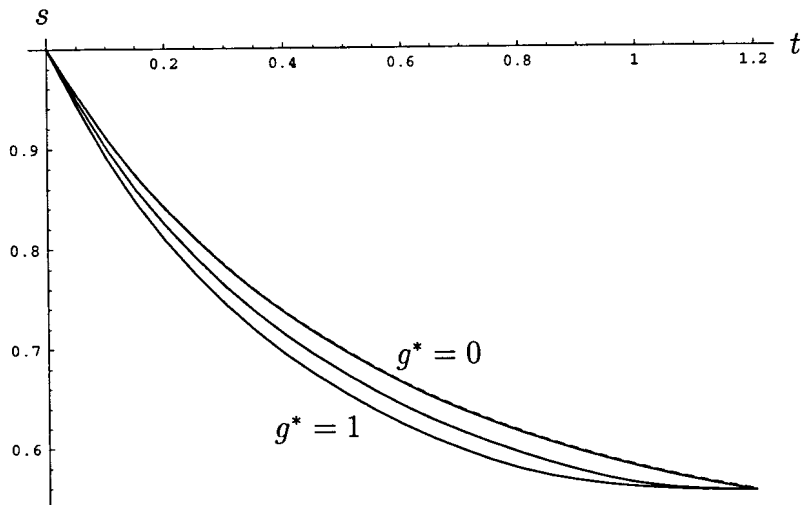


Figure 6: Height of paste $s(t)$ versus t for $\alpha_0 = 0.5$, $\alpha_c = 0.9$, $k = 1$ and $g^* = 0, 0.5, 1$. The dashed line shows the exact solution for $g^* = 0$.

observations.

It is interesting to compare the effect of varying k with that of varying g^* . In figure 6, we plot $s(t)$ versus t , keeping k fixed at 1 and varying g^* . Once again, the known exact solution (for $g^* = 0$) is plotted as a dashed line and is virtually indistinguishable from the numerics. We see from the figure that although the details of the evolution of α may depend on g^* to a certain extent, the broad characteristics of the air expulsion process, and in particular the behaviour of s (which is all that can be measured in the experiment), are almost independent of g^* . This is another reason to believe that the $g^* = 0$ limit is a relevant and useful approximation in practice.

5 Revised comparison with experiment

To compare with the experiment we must solve the heat-transfer problem and include variations of viscosity with temperature. As noted in section 4, if the heating is uniform and the cylinder is insulated top and bottom, then the temperature (averaged across the cross section), and hence the effective viscosity μ_2 , can be assumed to depend only on t . The resulting problem for T_2 was solved in Fitt & Howell (1998); we simply quote the necessary results here. The initial paste temperature and oven temperature are denoted by T_0 and T_f respectively. On the boundary of the cylinder a Newtonian heating law of the form

$$T_{2r} = h(T_2 - T_f),$$

is assumed, where $h < 0$ is a heat-transfer coefficient that depends on the type of convection present in the oven. Under these assumptions, the cross-sectionally-averaged temperature is given, in dimensional variables by

$$\langle T_2 \rangle = T_f + (T_0 - T_f) \sum_{k=0}^{\infty} \frac{4a^2 h^2}{\eta_k^2 (a^2 h^2 + \eta_k^2)} \exp\left(-\frac{\eta_k^2 k_2 t}{\rho_2 c_{p2} a^2}\right), \quad (33)$$

where η_k ($k = 0, 1, 2, \dots$) are the zeroes of

$$\eta J_1(\eta) + haJ_0(\eta) = 0.$$

A relationship is also needed between the paste viscosity and the temperature. Unfortunately, the details of this relation for the paste used in the experiment are at present proprietary information. However, using the (incomplete) data available, Fitt & Howell (1998) proposed the Arrhenius-type law

$$\mu_2 = 0.80081 \times 10^{-6} \exp\left(\frac{9834}{T}\right), \quad (34)$$

as a reasonable approximation in the temperature range of interest, where μ_2 is measured in Pa s and the temperature in Kelvin.

For given h and thermal parameters, μ_2 may now be regarded as a known function of time using (34) and (33). Of course, if further information becomes available (34) may need to be changed.

To carry out a complete comparison with experiment, the relevant dimensional parameters of the paste need to be determined. Again, our information about paste properties is far from complete, but the values shown in table 1 seem to be fairly realistic. It is worth commenting on the reliability of the data; the paste density, cylinder radius, cylinder height, applied load and gravitational acceleration are all either known or come from direct experimental measurements and can therefore be relied upon as being accurate data. The initial and critical paste volume fractions are inferred from the experimental results. The initial and oven temperatures may contain some inaccuracies, but are thought to be close to the truth. The thermal conductivity and specific heat of the paste are less reliable (in reality these parameters are probably functions of temperature anyway) but over the temperature ranges considered are probably not too much in error. The heat transfer coefficient h is highly speculative.

To compare with the experimental data (we have data for two experiments carried out under identical conditions; experimental points are shown using symbols) we consider three distinct cases:

(i) A full solution of the problem discussed in previous sections with $g^* = 0.34$ and $k = 1$. (This value for g^* is the correct one for the experiment.

Property	Symbol	Approximate Value	Units
Density	ρ_2	1570	Kg m^{-3}
Specific heat	c_{p2}	900	$\text{J Kg}^{-1} \text{K}^{-1}$
Thermal conductivity	k_2	2.5	$\text{W m}^{-1} \text{K}^{-1}$
Cylinder radius	a	8.5	cm
Cylinder height	L	30	cm
Applied load	M	31	Kg
Gravitational acceleration	g	10	m s^{-2}
Initial temperature	T_0	20	$^{\circ}\text{C}$
Oven temperature	T_f	100	$^{\circ}\text{C}$
Heat-transfer coefficient	h	~ -1	m^{-1}
Initial paste fraction	α_0	0.45	—
Critical paste fraction	α_c	0.91	—

Table 1: Estimated dimensional parameter values for the Elkem experiment

As far as k is concerned, we conjecture that k cannot exceed the value of $4/3$ that it assumes in the case of spherical voids. ($k = 1$ therefore seems to be a reasonable guess.) To effect this comparison, the non-dimensional piston height s is calculated as a function of t using a simple MATHEMATICA programme to perform the calculations outlined in the appendix. Time is then rescaled according to

$$t^* = \frac{Mg}{2\pi a^2} \int_0^t \frac{dt'}{\mu(t')}, \quad (35)$$

the necessary calculations being carried out using a simple FORTRAN code. (Although a different MATHEMATICA calculation must be carried out for each different value of k , the viscosity/temperature law conveniently changes the results for a given k only through (35).)

(ii) The case when $k = 1$ but $g^* = 0$, so that the solution (26) and (27) may be used. (For evaluation of these predictions, the easiest way to proceed is to solve (26) for given k and α_0 , producing a value of s for each required t . Time is then rescaled as in (i) above to give s and hence the effective density).

(iii) The model previously proposed in Fitt & Howell (1998) which corresponds to $g^* = 0.34$ and $k = 0$.

Figure 7 shows these results for a non-dimensional heat transfer coefficient $ah = -0.05$ (and thus $h = -0.588/\text{m}$). The times t_c and t_f were found to be 7624 and 8231 seconds respectively. Temperature and dynamic viscosity (scaled by 10^{-6}) are shown in the bottom portion of the figure. We note that for the new model the predicted density rise is slower, and in general

the agreement with experiment is poorer than for the original model. Also, (as expected) the calculations for $g^* = 0$ give very similar results to those for $g^* = 0.34$. For this set of comparisons however, the heat transfer coefficient is rather small; indeed we note that by the time the experiment has effectively finished the temperature has risen from the initial 20°C to only about 50°C.

Figure 8 shows results for a non-dimensional heat transfer coefficient $ah = -0.15$ (and thus $h = -1.76/\text{m}$). The times t_c and t_f were found to be 4358 and 4631 seconds respectively. Again, temperature and dynamic viscosity (scaled by 10^{-6}) are shown in the bottom portion of the figure. In this case, by the time the experiment has effectively finished the temperature has risen from the initial 20°C to about 80°C, which seems to be more realistic. Now the new model seems to agree better with the data, though in the late stages of the process it still predicts effective density rises that are too rapid. Again, the calculations for $g^* = 0$ give very similar results to those for $g^* = 0.34$. We note also that for this case the viscosity seems to decrease very rapidly. *It is almost certainly possible to greatly improve the quality of the model predictions by changing the viscosity law (34).* Since this amounts merely to guesswork, however, we have not done so here.

Overall, we conclude that the computations give results rather as expected; the old ($k = 0$) model predicts effective density rises that are too quick unless the heat transfer coefficient is chosen to be rather low. The results when $k = 1$ but g^* is taken to be zero are in all cases very similar to those when the correct value of g^* is used.

It must be emphasized that the results depend crucially on the viscosity/temperature relationship that is used, and in the computations above this is based largely on informed guesswork. If the model is ever to be properly validated, then the specification of an accurate μ vs. T law is vital.

6 Conclusions

In this paper, we have presented a two-phase model for the flow of the paste/air mixture in the Elkem experiment. The model is a generalisation of that proposed in Budd (1997), and seems to have the potential to give markedly improved agreement with experimental results. It is therefore reasonable to expect that it could be used as the basis of a predictive model of realistic electrode configurations. Such a model would have to include coupled electrostatic and thermal calculations in two or three spatial dimensions, and would clearly have to be solved numerically. However, great simplification is achieved by using an averaged two-phase approach rather than direct numerical simulation of each of the phases and the complicated interface

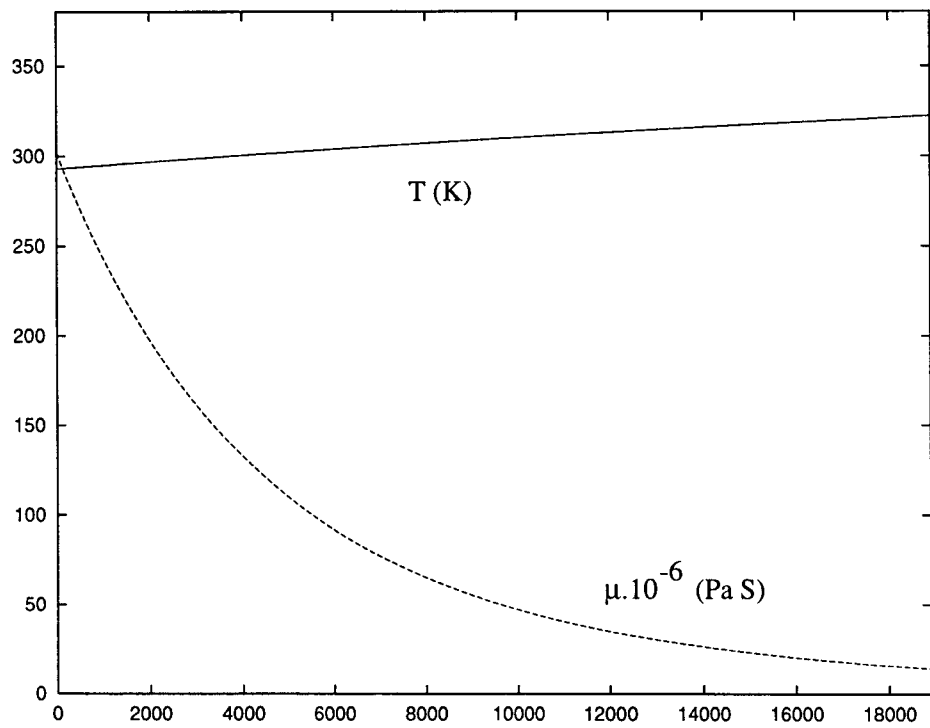
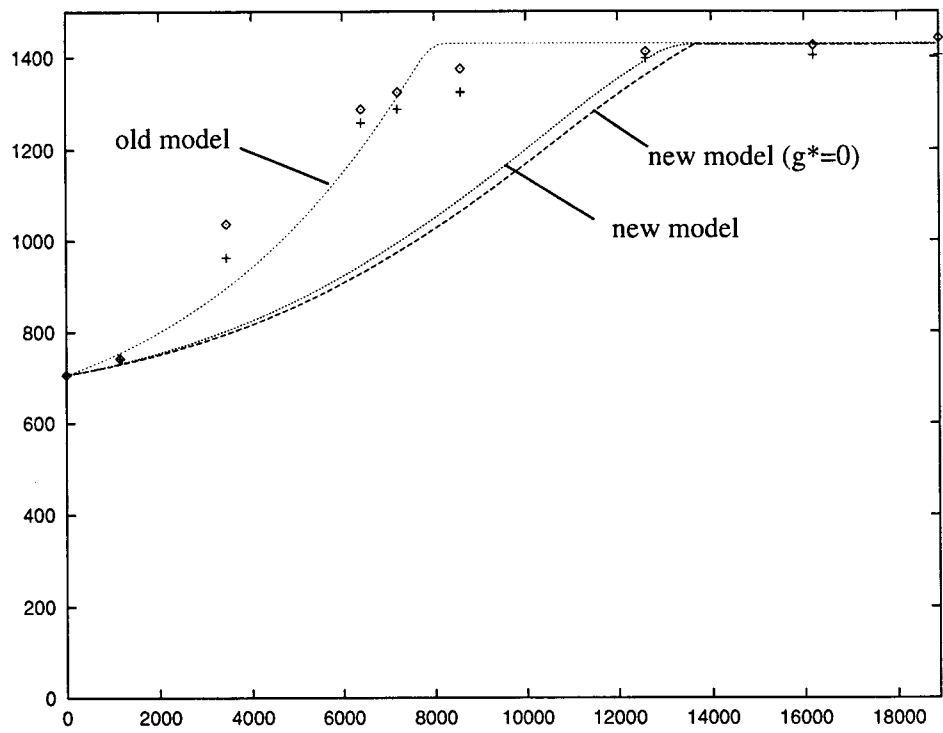


Figure 7: Comparison ($ah = -0.05$) between the old and the new model, (top), temperature (K) and viscosity $\mu \cdot 10^{-6}$ Pa S (bottom)

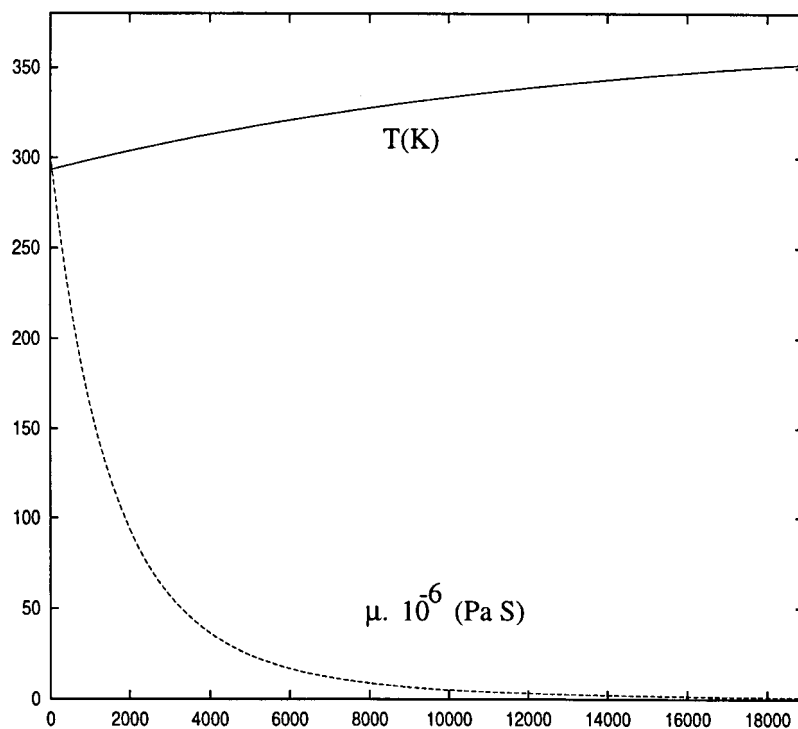
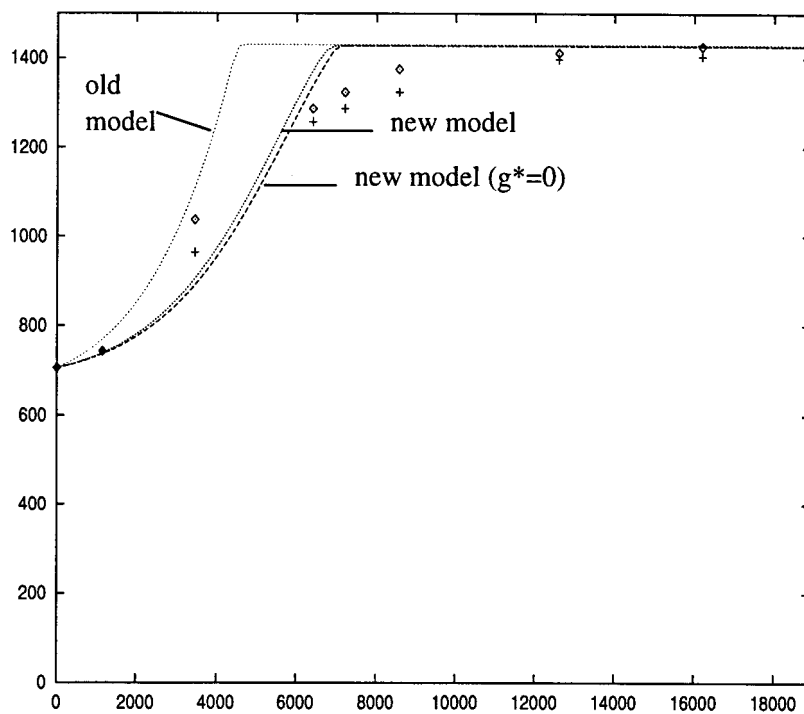


Figure 8: Comparison ($ah = -0.15$) between the old and the new model, (top), temperature (K) and viscosity $\mu \cdot 10^{-6} \text{Pa S}$ (bottom)

between them.

The model has a particularly novel feature that could make any non-trivial numerical calculations quite challenging, namely the switch between regime I and regime II. In the simple one-dimensional calculations carried out in section 4, this does present too much difficulty since the region of regime II could easily be located at the bottom of the cylinder. In a more general configuration, however, isolated pockets of regime II might appear and then convect around with the surrounding flow. Although this could lead to challenging computational problems, it could also give rise to some very interesting results.

The difference between the model presented here and that proposed in Budd (1997) centres on the notorious “equal pressures” assumption. This arises from the fact that the equations of two-phase flow in their most general form are underdetermined, so that some kind of closure assumption is needed to reduce the number of unknowns. In the absence of any evidence to the contrary, it has become common practice to do so by setting the phasic pressures equal to each other. Although for inertia-dominated flows this can lead to ill-posed problems (see Fitt (1996)), for slow-flow problems like that considered here, it has been found in the past to give reasonable results. In any case, in order to get a closed system of equations one has to assume *something*.

In this paper, we have followed an alternative route. By considering some simple sub-problems in which the interface between the two phases can be tracked exactly, we derived a constitutive relation (10) between the inter-phase pressure difference and the rate of air expulsion. This introduces a new constitutive parameter k , which may be regarded as an effective bulk viscosity of the mixture — the classical model with equal pressures is recovered if $k = 0$. In this light, we might regard the purpose of the Elkem experiment as being to determine the value of k for the paste/air mixture, so that the model can then be applied to a real electrode.

This alternative to the equal-pressure assumption and the modelling carried out here may well be applicable to many other two-phase industrial processes.

Finally, we stress once again the need for realistic viscosity/temperature data. In the absence of such information, the model is merely a mathematical invention; if sound data were available then it could become a valuable working model.

References

1. A.D. Fitt & P.D. Howell, The manufacture of continuous smelting electrodes from carbon paste briquettes, *J. Engng. Maths* to appear (1998).
2. A.D. Fitt, Mixed systems of conservation laws in industrial mathematical modelling. *Surv. Math. Ind.* **6** (1996) 21-53.
3. C.J. Budd, *Proceedings of the 1997 European Study Group with Industry*. University of Bath (1997).

Appendix: Numerical solution of the free-boundary problems

Before solving the free-boundary problem (19–24) numerically, it is convenient to recast it in Lagrangian form. Having set $\mu_2 = 1$ (see remarks in section 4.1), we define Lagrangian variables ξ and τ by

$$\xi = \int_0^z \frac{\alpha(z', t) dz'}{\alpha_0}, \quad t = \tau, \quad (36)$$

so that the chain rules relating Eulerian and Lagrangian frames are

$$\frac{\partial}{\partial z} = \frac{\alpha}{\alpha_0} \frac{\partial}{\partial \xi}, \quad \frac{\partial}{\partial t} = \frac{\partial}{\partial \tau} - \frac{w\alpha}{\alpha_0} \frac{\partial}{\partial \xi}. \quad (37)$$

From (19) we obtain

$$w_z = -\frac{\alpha_\tau}{\alpha}, \quad (38)$$

and α satisfies the hyperbolic equation

$$\left(2 + \frac{k}{1-\alpha}\right) \alpha_{\xi\tau} + \left(\frac{k(2\alpha-1)}{\alpha(1-\alpha)^2}\right) \alpha_\xi \alpha_\tau + 2g^* \alpha_0 = 0. \quad (39)$$

The boundary and initial conditions for (39) are

$$\left(2 + \frac{k}{1-\alpha}\right) \alpha_\tau = 2 \quad \text{on } \xi = 1, \quad (40)$$

$$\alpha = \alpha_0 \quad \text{on } \tau = 0. \quad (41)$$

We integrate (39) with respect to ξ , using the integrating factor

$$I = \left(2 + \frac{k}{1-\alpha}\right) \left(\frac{2(1-\alpha)+k}{\alpha}\right)^{\frac{k}{2+k}}, \quad (42)$$

to obtain

$$I\alpha_\tau = 2g^*\alpha_0 \int_\xi^1 \left(\frac{2(1-\alpha)+k}{\alpha}\right)^{\frac{k}{2+k}} d\xi' + 2 \left[\left(\frac{2(1-\alpha)+k}{\alpha}\right)^{\frac{k}{2+k}} \right]_{\xi=1}. \quad (43)$$

Our method is simply to timestep forward, updating α using (43). At any time, α can be plotted against z using

$$z(\xi, \tau) = \int_0^\xi \frac{\alpha_0 d\xi'}{\alpha(\xi', \tau)}. \quad (44)$$

As in section 4.3, we define t_c to be the time at which α first reaches its critical value α_c . This occurs at the bottom of the cylinder $\xi = 0$ and so t_c is the solution of

$$\alpha(0, t_c) = \alpha_c. \quad (45)$$

Also, we define t_f to be the time at which the whole process stops with $\alpha = \alpha_c$ everywhere. As in section 4.3, this is independent of g^* , and is given by

$$t_f = \alpha_c - \alpha_0 + \frac{k}{2} \log \left(\frac{1-\alpha_0}{1-\alpha_c} \right). \quad (46)$$

For τ between t_c and t_f there is a region, say $0 < \xi < \lambda(\tau)$, in which $\alpha = \alpha_c$ and there is no flow. However, because of the “top-down” nature of the integration carried out above, the solution for α obtained from (43) remains valid for $\xi > \lambda$. In practice we simply use (43) to evaluate α for $0 \leq \tau \leq t_f$; the difference between $\tau < t_c$ and $\tau > t_c$ only arises in the reversion from (ξ, τ) to (z, t) . The general solution procedure is as follows.

1. Evaluate t_f from (46).
2. Use (43) to find $\alpha(\xi, \tau)$ for $0 \leq \tau \leq t_f$.
3. Find t_c by solving (45).
4. For $\tau < t_c$, $\alpha = \alpha(\xi, \tau)$ and z is given by (44).
5. For $\tau > t_c$:
 - (a) Find $\lambda(\tau)$ such that $\alpha(\lambda(\tau), \tau) = \alpha_c$. (Note that $\lambda(t_c) = 0$.)

(b) For $0 < \xi < \lambda$ (i.e., $0 < z < \alpha_0 \lambda / \alpha_c$), $\alpha = \alpha_c$.

(c) For $\xi > \lambda$, $\alpha = \alpha(\xi, \tau)$ and

$$z = \frac{\alpha_0 \lambda}{\alpha_c} + \int_{\lambda}^{\xi} \frac{\alpha_0 d\xi'}{\alpha(\xi', \tau)}.$$

Report written by A.D. Fitt & P.D. Howell